JGR Earth Surface

RESEARCH ARTICLE

Key Points:
- Shore-normal winds are accelerated across a vegetated foredune slope but are accompanied by an onshore reduction in aeolian mass flux
- Sediment transport at the dunefoot and crest is governed by fetch and transport limitations respectively
- Foredune growth and recovery is thus strongly influenced by wind direction and vegetation cover

Correspondence to:
C. Schwarz,
cschwarz@udel.edu

Wind and Sand Transport Across a Vegetated Foredune Slope

C. Schwarz[1,2] , C. van Starrenburg[1,3], J. Donker[1,4] , and G. Ruessink[1]

[1]Department of Physical Geography, Faculty of Geosciences, Utrecht University, Utrecht, the Netherlands, [2]Now at School of Marine Science and Policy, University of Delaware, Lewes, DE, USA, [3]Now at Department of Estuarine & Delta Systems, Royal Netherlands Institute for Sea Research, Yerseke, the Netherlands, [4]Now at Geodan, Amsterdam, the Netherlands

Abstract Vegetated foredunes are widespread aeolian landforms along wave-dominated sandy coasts. In contrast to previous advances in dune erosion during storm surges, there is a little empirical data and understanding of aeolian processes during foredune recovery and growth. Based on a comprehensive data set (airflow, sand transport, topography change, and vegetation cover) collected across a steep (1:2.5, 21.8°), high (20 m) foredune during a windy 5-week period at Egmond aan Zee, the Netherlands, we demonstrate in agreement with previous studies that shore-perpendicular winds accelerate by a factor of 3 from dune foot to crest but result in low aeolian mass fluxes that are maximum at the dunefoot, favoring local deposition. In contrast, oblique and alongshore winds up the foredune are accelerated less (or even decelerate) but are important in bringing sand from the dunefoot on to the foredune slope, where it is deposited when vegetation cover exceeds about 50% of the maximum density measured on the dune crest. Moreover, our data suggest that sediment flux at the dune foot is limited by fetch-induced sediment availability, whereas sediment flux at the dune crest is limited by transport capacity, which depends on the wind velocity and the distance traveled over vegetation. Our study thus highlights the importance of wind direction and vegetation cover to foredune growth and recovery.

1. Introduction

Coastal foredunes, the most seaward shore-parallel sand dunes, constitute the primary barrier separating environments governed by marine (e.g., near-shore, beach) and terrestrial processes (e.g., back dunes) along sandy coasts. They arise where landward aeolian sand transport originating from the foreshore gets deposited within vegetation on the backshore (Davidson-Arnott et al., 2018; Hesp, 1989, 2002; Zarnetske et al., 2012). Their evolution depends on trade-offs between nearshore processes such as sand availability from the beach, wind regime, sand removal due to storm-wave action, and sand stabilization by terrestrial vegetation (Cohn et al., 2018; Davidson-Arnott & Law, 1996; P. Hesp, 2002; Psuty, 2008; Short & Hesp, 1982).

At the beach, wind velocity and local grain-size characteristics control instantaneous dry sand transport (e.g., Bagnold, 1954). Therefore, sand availability can be limited through processes such as armoring (Hoonhout & Vries, 2016), moisture content (Davidson-Arnott et al., 2005) and fetch limitations (i.e., the downwind distance from the location of transport initiation to the beach-dune transition is too small for the transport to reach its potential wind-speed dependent maximum) (Bauer & Davidson-Arnott, 2002; Delgado-Fernandez, 2010, 2011; Hage et al., 2020). At and across the foredune, wind velocity and consequently sand transport is strongly controlled by the interaction between regional wind flow and surface topography (topographic steering) which in turn has major implications for foredune growth. Previous work demonstrated that winds approaching the foredune in an oblique angle tend to be deflected toward crest-normal along the stoss (upwind) slope, where the degree of deflection depends on the incident angle as well as the height above surface. Hereby, the lowest streamlines were shown to experience the greatest degree of deflection (P. A. Hesp et al., 2015; Walker et al., 2017). Crest-perpendicular winds were shown to decelerate at the foredune foot and accelerate up the stoss slope (due to dilated streamlines at the dunefoot and streamline compression at the crest), if the foredune is sufficiently high and flow detaches from the crest (e.g., Bauer et al., 2012; W. De Winter et al., 2020; P. A. Hesp et al., 2015; Smyth et al., 2012; Walker et al., 2009). During strong winds this flow acceleration toward the crest was shown to result in sand transport high enough to be able to reach the lee-side (downwind) of the foredune (Arens et al., 1995; Hesp & Walker, 2013). Highly

oblique winds (further referred to as alongshore) were shown to be deflected parallel to the crest line (Bauer et al., 2012). For these alongshore winds the reduction in mean wind speed at the dune foot and acceleration toward the dune crest was shown to be less pronounced due to declining effects in flow stagnation and streamline compression over the effectively less steep dune slope (Arens et al., 1995). This can often result in increased sand transport along the beach rather than onto the foredune. However, increased drag due to the vegetated surface at the lower stoss slope can also produce a decrease in wind speed and topographic steering toward the foredune foot which may enhance sand transport form the upper beach onto the lower foredune stoss slope. Moreover, vegetation drag also decreases sand transport across the dune slope thereby creating a disparity between transport observed at the stoss slope and at the beach (Walker et al., 2017). The above examples show that wind direction and dune morphology exert an important impact on wind speed and direction and consequently dune growth.

In addition to beach processes, terrestrial vegetation, such as marram grass, exerts a major influence on the morphological evolution of foredunes. Vegetation tends to fix the foredune in place (P. Hesp, 2002; Maun, 2009) through its capacity to promote sand deposition and reduce erosion (e.g., Davidson-Arnott et al., 2012; Maun, 1998). Sand deposition is promoted since vegetation reduces the wind velocity, facilitating the deposition of wind-entrained sand grains. Sand erosion is reduced due to vegetation sheltering the sand surface from wind- and wave-generated shear stress and thus reducing particle entrainment (e.g., Carter & Stone, 1989; Davidson-Arnott et al., 2012; P. Hesp, 2002). In the context of existing foredunes, as described above, vegetation slows down airflow across their stoss slope, which constitutes an additional factor shaping foredune topography. Although in many cases vegetation increases the surface roughness on the dune slope, it remains part of scientific debate how vegetation and foredune morphology influence foredune development (e.g., Arens et al., 1995; P. A. Hesp et al., 2005; Walker et al., 2009). For instance, Duran and Moore (2013) suggested that vegetation controls the maximum size of coastal dunes assuming that growth in dune height is limited by the emergence of a flow stagnation zone at the seaward base of the foredune caused by steepening of the stoss slope via sediment deposition from the nearshore consequently, cutting off sand supply to the stoss-slope and crest of the foredune. However, Davidson-Arnott et al. (2018), after further investigating this phenomenon through field observations, put forward that this suggestion does not hold true for real foredune systems. Therefore, Davidson-Arnott et al. (2018) further suggested, unsteady multidirectional nonuniform flow conditions, cause sediment transport onto the stoss slope and crest regardless of critical stoss-slope steepness (e.g., P. A. Hesp & Smyth 2016b). Davidson-Arnott et al. (2018) considered this a result of a large proportion of annual total transport into most foredunes taking place under oblique and alongshore winds, during which adverse pressure gradients on the windward side are not as pronounced allowing transport toward the crest. Moreover, Arens (1996) has shown that the interaction between vegetation and topographic steering, can also result in reduced sand transport to the upper stoss-slope, thus potentially limiting maximum foredune height (Arens, 1996). Vegetation type and vegetation density were also shown to have important implications on foredune growth, since vegetation type affects vegetation density and moreover determines the plant's response to sedimentation ranging from growth to die-off. For instance, dense vegetation, with stimulated growth through sedimentation, leads to enhanced deposition instigating higher foredunes than sparse vegetation, respectively (e.g., P. Hesp, 1989; Maun, 1998).

Since foredune growth is strongly influenced by topographic steering, both scarping of the foredune front during storms altering foredune form and vegetation cover strongly affect sediment transport (e.g., in 2014, Figure 1; De Winter et al., 2015; Ruessink et al., 2019). For instance, during post-storm recovery scarps fill up by wind-blown sand deposited at the dune foot, building a so-called dune ramp (e.g., Carter et al., 1990, Ollerhead et al., 2013), altering sediment transport and deposition patterns across the foredune. Previous studies used numerical models to compare flow deflection across a scarped and nonscarped foredune, with uncertain implications on dune recovery (Hesp & Smyth, 2016a, 2019; Piscioneri et al., 2019). Volumetric field observations led to conceptual insights, showing that a dune ramp has a major impact on sand transported to the dune crest and lee slope, where scarped dunes devoid of a dune ramp show significantly reduced crest directed transport (Castelle et al., 2017; Christiansen & Davidson-Arnott, 2004; Donker et al., 2018; Ollerhead et al., 2013; Figure 1). Long-term field observations were not able to explain sedimentation across the foredune in relation to vegetation cover and wind data (Keijsers et al., 2015).
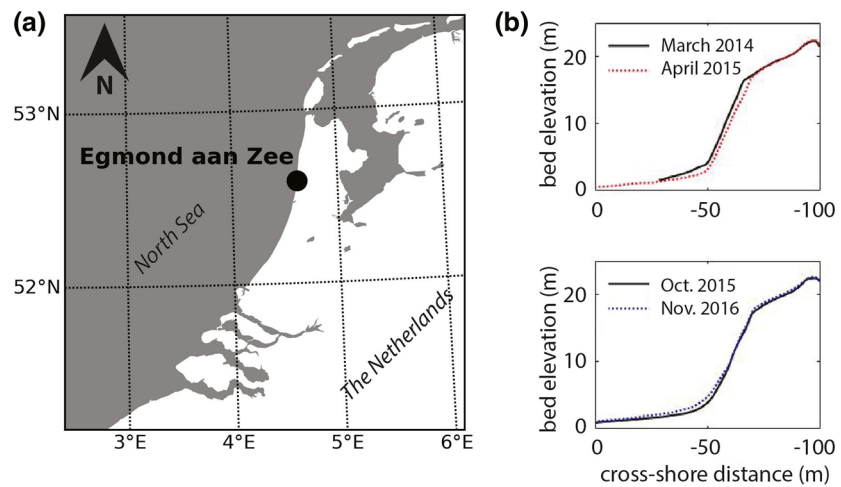
Figure 1. (a) Field site of foredune measurements near Egmond aan Zee (52.591033°and 4.614465°), the Netherlands; (b) development of the foredune profile between 2014 and 2016 showing from top to bottom one erosion events after a storm in October 14 (red) and 1 year of dune toe recovery without storm 2015–2016 (blue). The topographic data are from Ruessink et al. (2019).

Thus, most of our knowledge on the growth and recovery of scarped foredunes is based on volumetric analyses and conceptual pictures, but lack a detailed underpinning of the underlying aeolian processes. This study investigates the relative influence of sediment availability from the beach and vegetation altered transport capacity across the foredune on growth and recovery of a foredune at the coast of the Netherlands. We hypothesize that sediment deposition across the foredune is not only a function of vegetation cover and sediment input form the beach, but also governed by wind direction and topographic steering dependent transport paths across the vegetated foredune. We analyze detailed measurements of aeolian sand flux, wind variables (speed, direction, and turbulence) and vegetation and compare them to high-resolution topographic datasets. Measurements were gathered during a field campaign in October 2017 at the ~20 m high foredune near Egmond aan Zee, the Netherlands. Results provide field evidence demonstrating the complexity inherent to near-surface sand transport responses across foredunes and show the importance of wind directions and vegetation cover in governing foredune growth.

2. Materials and Methods

The current study focuses on the 20-m foredune at Egmond aan Zee in the high-wave North-Sea environment. This field site represents an ideal test case to study foredune growth in respect to wind magnitude, direction, sediment transport and vegetation cover, because the steep and high foredune is expected to cause pronounced wind direction depending topographic steering and altered sediment transport. Field data were collected during a 5-week period (02 October 2017 to October 31 2017) near Egmond aan Zee (52.591033° and 4.614465°) (hereafter referred to as Egmond), the Netherlands (Figures 1 and 2). Wind direction, magnitude and turbulent kinetic energy (*TKE*) were continuously recorded across the foredune using three 3D ultrasonic anemometers (Figure 2). Sand transport was quantified across the foredune at 5 days (5, 6, 11, 17, and 25 October) using sediment catchers (Figure 2). Vegetation was quantified along a study transect through a one-time assay at the beginning of the study period.

2.1. Study Area

The study area is located at the Dutch North Sea coast south of Egmond (Figure 1a). The coast is approximately north-south oriented, with an inclination of 8° relative to north. Although nourishments have been carried out north and in front of Egmond (e.g., Van Duin et al., 2004), the study site is relatively undisturbed. The studied cross-shore transect was 20 m south of the beach pole with km-indication 41.00 (52.591033°and
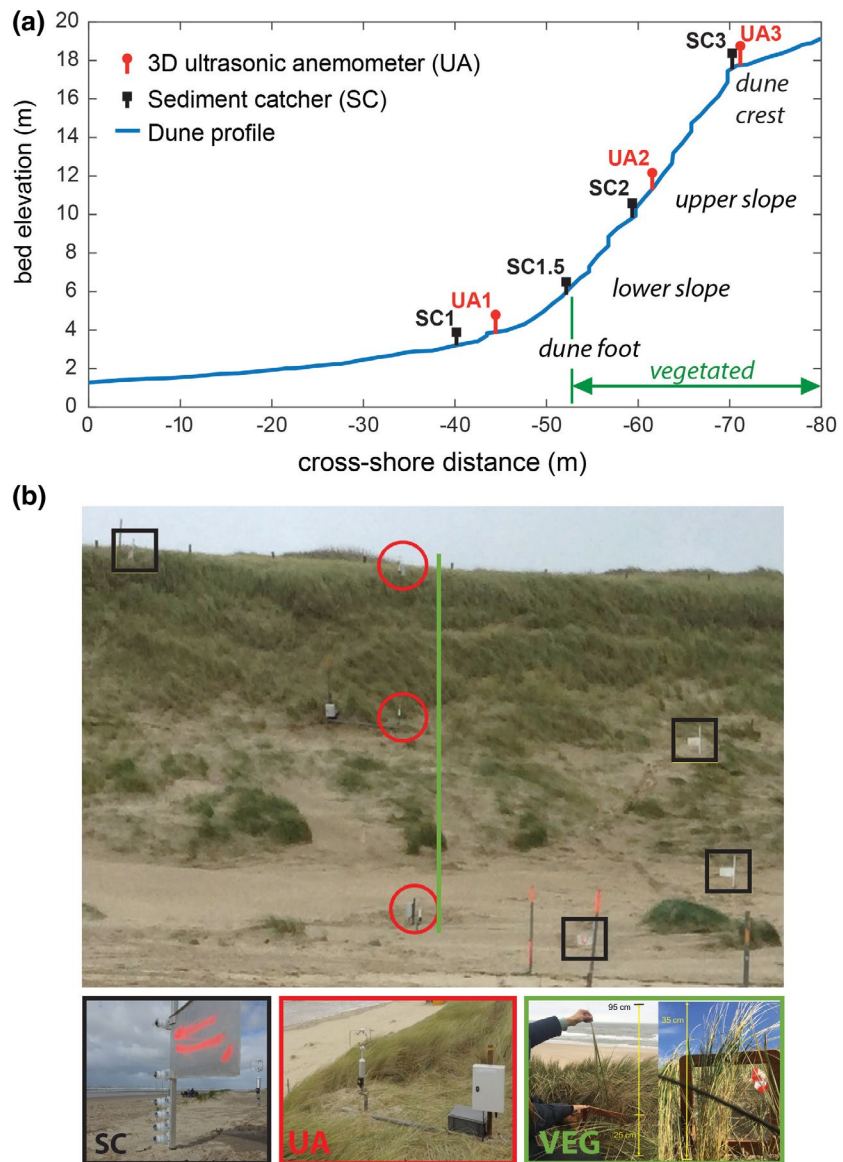
Figure 2. a) Field measurement setup across the foredune, UA: 3D ultrasonic anemometers, SC: modified Wilson and Cook sediment catcher array, we further refer to the change in slope as the crest measurement position, although the highest point is located further landward. Panel (b) shows a frontal view of field measurements setup using the same abbreviations as above, VEG indicates the location of the vegetation transect.

4.614465°). The ~75 m wide intertidal beach has a low slope of on average 1:40 (1.43°) and is subjected to a microtidal semi-diurnal tidal fluctuation with a spring tidal range of just below 2 m. The mean grain size at the beach is approximately 0.25 mm. The beach is wave-dominated and exposed to waves mainly approaching from southwest to northern directions (Aagaard et al., 2005). The annual average offshore significant wave height is 1.3 m (years 1999–2011) (De Winter et al., 2015). The area is characterized by a lateral continuous foredune of about 20 m high with a steep stoss slope of 1:2.5 (21.8°) because of occasional erosion events (Figures 1 and 2). The foredune vegetation is dominated by European marram grass (*Ammophila arenaria*), whereas the lower dune foot is characterized by a mixture of marram grass, sand couch grass (*Elytrigia juncea*) and lesser hawkbit (*Leontodon saxatilis*) (Arens et al., 2002). Southwest wind direction is dominant, with maximum velocities of 25 m s^{-1} which is obliquely onshore. October marks the beginning of the storm season, which generally lasts until February (Arens et al., 1995).

Table 1
Sediment Catcher Description From Foredune Foot to Foredune Crest (1–3), the Letters (A–F) Constitute the Height of the Sediment Traps Above Bed in Logarithmic Spacing, cmab (Centimeter Above Bed)

Trap height (cmab)	1	1.5	2	3
A	6.5	9.4	6.5	5.5
B	12.7	15.3	12.5	11.6
C	19.0	20.0	18.5	17.5
D	25.0	26.9	24.3	23.4
E	38.3	40.2	37.3	36.7
F	63.5	65.0	62.7	61.7

2.2. Field Measurements

Field measurements were collected across the stoss side of the foredune. Coordinates were recorded in local Dutch coordinate system RD2008, and where subsequently transformed in reference to the former Argus tower (X/Y/Z: 102572/511553/0, 277.2° relative to north), previously located next to beach pole 41.25 (Van Enckevort & Ruessink, 2001). All x-coordinates point negatively onshore and y-coordinates positively to the south, while z-coordinates are the elevation above Dutch ordnance level (NAP), which is approximately mean sea level. All coordinates are in meters. Axes of figures are reversed so that the seaside is orientated to the left-hand side (west) and north toward the magnetic north. The cross-shore dune and beach profile of the study transect, measured with a RTK-GPS on 31 October 2017, shows a gentle sloping beach (1:40 and 1.43°) and a steep stoss slope at the foredune (1:2 and 21.8°) that ends at ~18 m above mean sea level; it then continuous gently for another ~50 m to the dune crest at ~22 m above mean sea level (Figure 2). Incipient foredunes were present at the dune foot to the south of the transect (De Winter et al., 2020; Ruessink et al., 2019).

2.2.1. Wind Measurements

Three 3D Ultrasonic Anemometers, Model 81000RE, R.M. Young Company, further referred to as UAs (Figure 2), were deployed to measure wind flow. UAs measure three-dimensional wind velocity and direction, using the transit time of ultrasonic acoustic signals, from which absolute wind speed and direction can be calculated. From the speed of sound, the sonic temperature is also derived, corrected for crosswind effects. For a wind speed range of 0–30 m s^{-1}, it has a measurement resolution of 0.01 m s^{-1} and a *rms* error ±0.05 m s^{-1}. The three permanently installed UAs operated at a sampling frequency of 10 Hz during the entire campaign with small interruptions because of technical issues. The measurement volume of the UAs was at 90 cm from the ground (40 cm above the mean vegetation height at UA2 and UA3) and aligned to the beach pole of km-indication 40.75 ($x/y/z = -35.4/-501.2/3.4$ m) as reference.

2.2.2. Sand-Transport Measurements

To study aeolian sand transport across the dune, Modified Wilson and Cook sediment catchers were deployed (Sterk & Raats, 1996) (termed SC, Figure 2). The catchers trap moving material at six different heights above surface between 0.05 and 0.7 m. Each catcher consisted of six plastic bottles positioned at different heights in logarithmic spacing (Table 1). Each plastic bottle (approximately 100 ml) has two glass tubes (inner diameter = 8 mm and opening = 50.3 mm^2) that enter through the lid. One tube allows air and sediment to enter, while the other opening allows air to escape. The bottles were mounted on an aluminum wind vane freely rotating around a fixed pole to assure orientation in the wind direction. Literature reports the sediment catchers trapping efficiency range from 49% (Sterk & Raats, 1996), 54.4% (Sterk et al., 2012), 72%–87% (Dong et al., 2011) and up to 100% (Goossens & Offer, 2000). The currently used sediment catchers were tested in a wind tunnel experiment using sand from the above-mentioned field site which resulted in a trapping efficiency of 35% (De Winter et al., 2018). The catchers used here had a larger wind vane than those from Sterk and Raats (1996). Sediment traps were located at varying heights above surface (Table 1). The operating period was timed on the second and the content of the traps was weighted before and after drying in an oven for 24 h at 105 °C. Four sediment catchers were placed at fixed positions, which were chosen left and right of the cross-shore transect to not disturb the measurements of the UAs and to ensure free rotation of the wind vane (Figure 2). Sediment catcher deployments were carried out if wind speed was expected to exceed 10 m s^{-1} and no or little precipitation was predicted (5 deployments during study period: 5.10, 6.10, 11.10, 17.10, and 25.10 over periods from 1 to 6 h).

2.2.3. Morphology and Vegetation

Locations of the three ultrasonic anemometers (UA1, UA2, and UA3) and four sand catchers (SC1, SC1.5, SC2, and SC3) were measured using an RTK-GPS (Trimble). Morphological foredune changes were evaluated through two UAV-LIDAR surveys (Sensor HDL-32e) carried out by drone flights (Shore Monitoring and Research BV) before and after the campaign (September 23 2017 and November 03 2017, respectively),

resulting in elevation models, with 1 m cell size validated by RTK-GNSS measurements of the company. See Ruessink et al. (2019) for details on data acquisition and processing.

Plant density was estimated at the cross-shore transect at 1 m intervals by counting all individual stems within 5 adjacent 25 × 25 cm quadrants. Photographic documentation was taken for all counts on all transects. To account for natural deviations, rows of five quadrants were positioned per 1 m interval with the middle quadrants aligned with the study transect. Additional to the stem count, the width and length of representative stems was measured. For each quadrant the plant species were determined, and the dominant species recorded. The plant density was determined for each quadrant and corrected for the surface area resulting in stems per m^2. The mean of the five quadrants per cross-shore interval was used for further analysis. Due to the dense cover at the foredune crest, the vegetation cover in percentage could be determined relative to the coverage at the dune crest and the bare beach. The quadrant with the most numbers of stems at transect (upper slope/dune crest) was set as 100% as a reference.

3. Data Analysis

3.1. Wind

All data were preprocessed removing data with device error flags and filtering records with sonic temperature changes over 2 °C within 5 s, which indicates precipitation. The axes were chosen that u is the horizontal wind velocity in east-west direction (positive from east) and v is the horizontal wind velocity in north-south direction (positive from north). The velocity component w is the vertical wind velocity (positive from below). Consistent with data processing by the Royal Netherlands Meteorological Institute KNMI, the instantaneous 10 Hz time series of u, v, and w were first smoothed into series of 3-s running means. The mean wind velocity ($\overline{u}$, $\overline{v}$, and $\overline{w}$) and wind direction (θ) were then computed as 10-min averages based on the running means, while the TKE was computed using the nonsmoothed wind data. A visual quality control of the data for each deployment day was conducted for the 10-min averages, looking for sudden jumps in wind velocity components to avoid the inclusion of disturbed measurements, for example, due to maintenance.

The following equations were used to obtain the total wind speed (U), the TKE and the wind direction (θ). The wind speed was based on the mean wind components $\overline{u}$, $\overline{v}$, and $\overline{w}$.

$$U = \sqrt{\left(\overline{u}^2 + \overline{v}^2 + \overline{w}^2\right)}. \tag{1}$$

The TKE was calculated as:

$$TKE = 0.5 * \left(\overline{\left(u'\right)^2} + \overline{\left(v'\right)^2} + \overline{\left(w'\right)^2} \right). \tag{2}$$

Whereby TKE as calculated by the mean (indicated by an overbar) of the square of the fluctuating part of the velocity components (indicated by a prime [u',v',w'], i.e., $u' = u - \overline{u}$, etc.). The wind direction was obtained with North being 360°

$$\theta = \arctan\left(\overline{u,v}\right) * 180 / \pi. \tag{3}$$

Wind directions for $U < 2 \text{ ms}^{-1}$ were highly scattered and are not considered in the remaining of this study.

The dimensionless wind speed ratios between the UAs were used to express the change in wind speed relatively as increase or decrease, based on incipient wind direction. To compare the wind statistics to nondisturbed wind flows, data of a proximate offshore measuring station (IJmuiden lat.: 54.4693° lon.: 4.5204°, and wgs1984) were used as a reference. The used station is operated by the Dutch governmental organization Rijkwaterstaat, roughly 16 km south of the study site and about 1 km to the west of the southern IJmuiden harbor mole. To compare velocities between UA1 and the reference station, the IJmuiden wind velocity data were transformed from its measuring height of 10 m above surface to 0.9 m above surface using the law of the wall, assuming a logarithmic velocity profile. In this approach the shear velocity u_* was calculated using a roughness length of 8×10^{-6} m (= 1/30 d50 as proposed by Bagnold (1954); and the von Karman constant k was set to 0.41.

To study the development of turbulence across the foredune, the nondimensional ratio (*rts*) of the *TKE* and wind speed (*U*) was calculated,

$$rts = \frac{\sqrt{TKE}}{U}.$$

(4)

Wind directions were recalculated so that −90° represents alongshore southern winds, 0° perpendicular onshore, 90° alongshore northern winds and 180°/−180° perpendicular offshore. All wind directions were recorded and preprocessed, but offshore wind directions were excluded from further analyses. This was done due to the research goal in assessing wind and aeolian transport across the foredune, originating from the beach. The reference wind direction was, based on De Winter et al. (2020), assumed to be the same at 0.9 m and 10 m above surface.

3.2. Sand Transport and Morphology

For periods during which saltation measurements were conducted, the contents of the vertical sand traps were dried and weighted. From the weight and the noted operating time, the wind-blown mass flux per bottle in g m^{-2} s^{-1} was calculated as:

$$Q_b^{\bar{z}} = \frac{1}{A}\frac{m}{t},$$

(5)

whereby $Q_b^{\bar{z}}$ is the mass flux for each bottle at elevation *z*, *A* is the circular surface of the pipe opening (50.3 mm^2), *m* is the sediment caught in grams and *t* is the duration time of operation. Based on the sand mass flux of the six bottles, a vertical profile was drawn, and an exponential curve was fitted to it. For this, a best-fit model was used for each catcher. The fitted curve was then integrated vertically over the height of 0–1 m to obtain the total mass flux Q_m in g m^{-1} s^{-1} at the location of the catcher. The calculated mass flux was multiplied by the trapping efficiency factor of 1/0.35 (trapping efficiency 35%) (Ellis et al., 2009).

$$Q_m = \frac{1}{0.35}\int_0^m Q_b^{\bar{z}}\,dz$$

(6)

Additionally, the dune volume before and after the field work for the study transect was calculated. The UAV data were interpolated and integrated for the cross-shore length of the stoss side at the transect. The dune volume was calculated from the dune foot 2.5 m above sea level until the change in dune slope at the stoss side (e.g., Figures 1 and 2).

4. Results

4.1. Wind Measurements

During our measurement campaign wind velocities ranging from 0 to 25 m s^{-1} and wind directions from northern-longshore (+90°) to southern-longshore (−90°) were recorded (Figures 3 and 4). A comparison between conditions across the foredune (UA1-UA3) and the reference station (IJmuiden) reveals clear spatial differences in wind direction and magnitude (Figure 3). We will now describe and analyze observations comparing wind speed, wind direction and *TKE* across the foredune and with respect to the reference station. The magnitude of wind speeds at the dune foot, upper-slope, dune-crest and at the reference are further referred to as U_{UA1}, U_{UA2}, U_{UA3}, and U_{ref}, respectively. A similar nomenclature is used for other variables such as wind direction and *TKE*, dir_{UA1}, and TKE_{UA1}.

A comparison between foredune locations and the reference station shows that U_{UA1} and U_{UA2} were generally lower than U_{ref}, whereas the opposite could be observed at U_{UA3} (Figure 3). Wind acceleration across the foredune, U_{UA1} to U_{UA3}, was recorded up to a factor 3.1 (for wind directions between −14 and 8° cross-shore winds (Figures 4 and 5c). The acceleration from U_{UA1} to U_{UA2} was generally smaller (max. 1.5) than from the U_{UA2} to U_{UA3} (max. 2.2) (Figures 5a and 5b). What is more, flow acceleration was observed to be strongly dependent on the incoming wind direction consistent with findings for other sites in Arens et al. (1995) and Walker et al. (2017). From U_{UA1} to U_{UA2}, a maximum acceleration of 1.5 was recorded around onshore
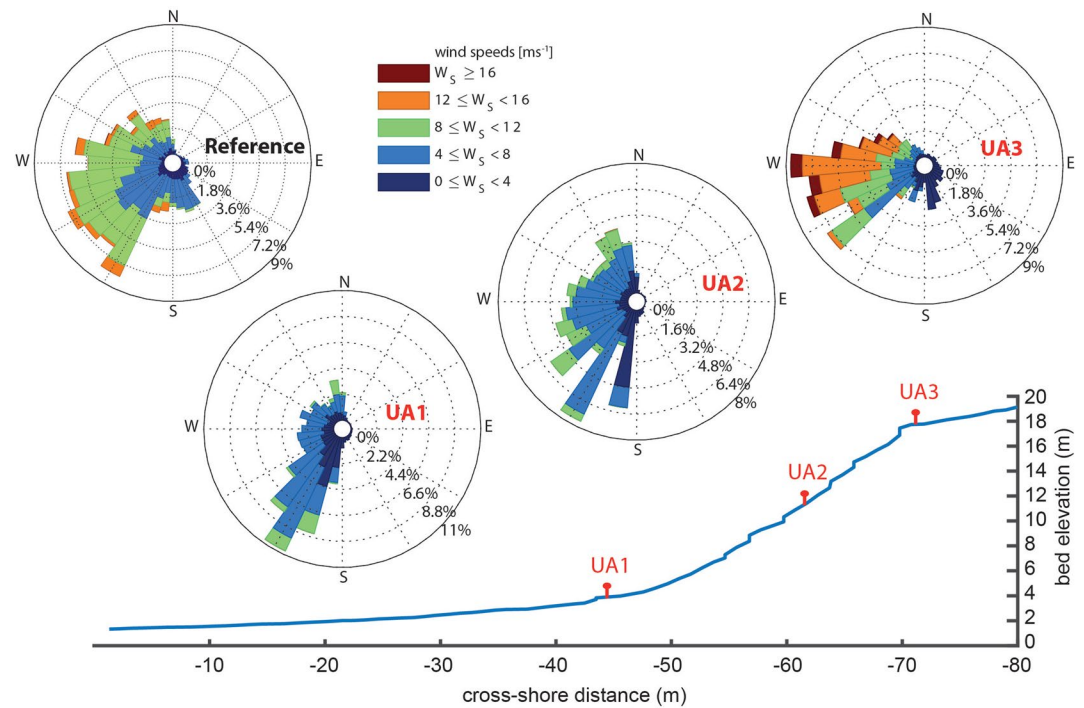
Figure 3. Wind rose measured at all three stations across the foredune (UA1-3) and the reference (station 225, IJmuiden) during the field campaign in October 2017; wind speeds at the reference were corrected to 0.9 m using law of the wall; the foredune is approximately N-S oriented, with W being onshore.

winds (−22°–14°), whereas highly oblique wind directions (−76° south and 60° north) led to deceleration (Figure 5a). From U_{UA2} to U_{UA3} wind speed was predominantly accelerated, with the maximum acceleration of >2 for onshore winds up to ±22° deviation from shore normal. Highly oblique onshore winds from the south led to an acceleration of 1.3, while highly oblique winds from the north decelerated wind by a factor of 0.8 (Figure 5b).
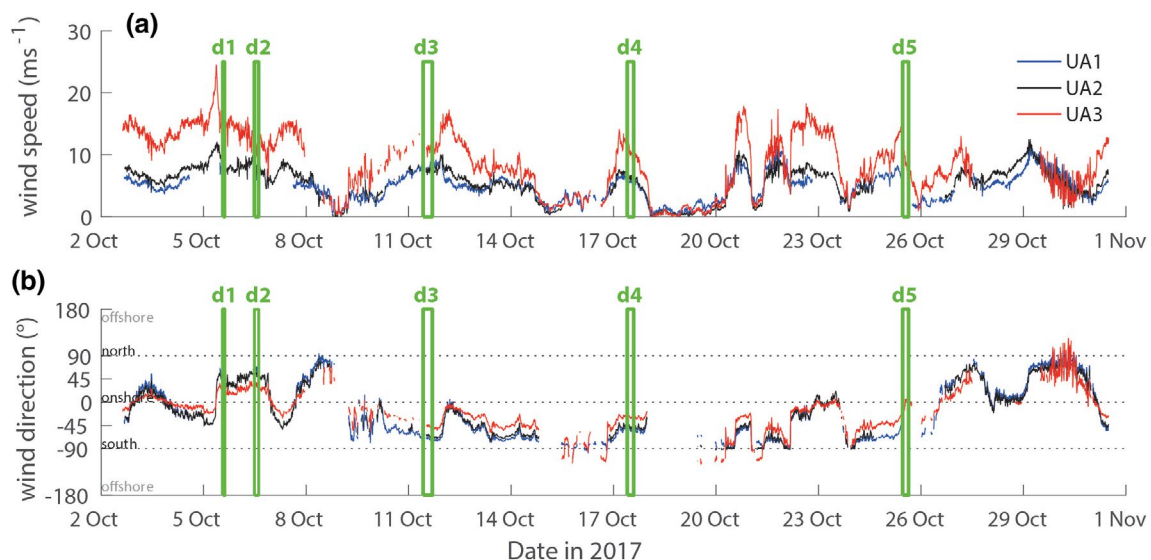

Figure 4. Time series of (a) wind speed and (b) directions over the deployment period in 2017; Green squares indicate periods where sediment catchers (d1–d5) were deployed, wind directions for velocities <2 m s^{-1} were removed due to high variability and being below the entrainment threshold.
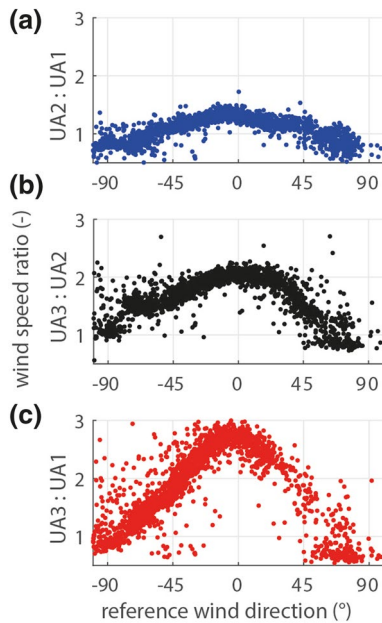
Figure 5. Ratios of wind speed at different stations (UA1, UA2, and UA3) across the foredune versus reference wind direction. (a) UA2:UA1, (b) UA3:UA2 and (c) UA3:UA1.

Not only wind magnitudes but also wind directions changed across the foredune. Wind directions at the dune foot were observed to rotate toward alongshore directions (dir_{UA1}, Figure 6a), whereas wind directions at the dune crest were observed to rotate toward shore-perpendicular directions (dir_{UA3}, Figure 6c). Like the wind magnitudes, deflection angles exhibited a dependency on the incoming wind direction consistent with findings in Arens et al. (1995) and Walker et al. (2017). This was foremost observed for dir_{UA1} and dir_{UA3}, with no clear direction dependency at UA2 (Figures 6d–6f). At UA1, maximum deflection angles of 25–65° were observed during oblique onshore wind directions. However, the observed deflection toward alongshore was more pronounced for north-western than for south-western winds, with the greatest deflection angles found for incident wind directions of 20–60° (Figures 6a and 6d). At UA3, the largest wind deflection angles of 20–65° toward shore-perpendicular were observed for highly oblique and alongshore winds (Figures 6c and 6f). While the data cloud was S-shaped for UA1, this trend was mirrored at UA3: the deflection toward alongshore at the dunefoot changed to a deflection toward shore-normal at the dune crest (Figures 6a–6f).

A comparison of *TKE* across the foredune locates the highest *TKE* values at the upper slope (TKE_{UA2}) and crest (TKE_{UA3}), and lower *TKE* values at the dune foot (TKE_{UA1}) (Figure 7). *TKE* increases with increasing wind speed at all UAs (Figures 7a–7c), however the rate of increase is strongly dependent on wind direction and location across the foredune. The rate of increase in TKE_{UA1} and TKE_{UA2} with wind speed shows little dependency on wind direction (Figures 7a and 7b). The rate of increase in TKE_{UA3} with wind speed, in contrast, shows that *TKE* for alongshore wind directions (exceeding ±60°) (Figures 7a–7c, dark red and dark blue) increases with a faster rate than for shore-perpendicular winds (Figure 7c, shades of green, yellow, and light-blue). The dimensionless ratio, between $\sqrt{TKE}$ and *U*, *rts* also showed little dependence on wind velocity (not shown), but a clear dependency on wind direction. Onshore winds resulted in high rts_{UA1}, while highest values at rts_{UA2} and rts_{UA3} were observed during alongshore winds (Figures 7d–7f). Turbulence is thus strongest (relative to U) during onshore winds at the dunefoot, and during shore-parallel winds higher up on the foredune.

4.2. Sand Transport

Sand transport varied considerably across different locations on the foredune and measurement days (d1–d5) (Figure 8). During oblique (d1 and d4) and alongshore wind directions (d2 and d3) the maximum depth integrated mass flux was recorded at location SC1.5 (lower slope), with alongshore wind conditions generally exhibiting a higher depth integrated mass flux at SC1.5 than oblique wind conditions (Figure 8f). During shore-perpendicular wind directions (d5) a decrease in depth integrated mass flux (g m^{-1} s^{-1}) across the foredune was observed (Figure 8e), despite the strong observed acceleration in wind magnitude (Figure 5). Moreover, measured sand transport profiles show that during alongshore wind conditions higher saltation heights were observed than during oblique wind conditions (Figures 8a–8d), with the lowest saltation heights during onshore winds (Figure 8e). The average depth integrated fluxes during all deployments relative to the dune foot (SC1, 100%), show an increase in mass flux at the upper dune foot to 305% just below the vegetation edge (SC1.5), subsequently dropping to 16.8% half way on the dune slope (SC2) and reaching its minimum on the dune crest (1.4%) (SC3) (Figure 9). The largest average mass flux at SC1.5 reflects the dominance of obliquely to alongshore wind approach angles in our data set (d1–d4). During these conditions longer fetch distances upwind of the dune line potentially led to higher transport at SC1.5 (Bauer & Davidson-Arnott, 2002). When comparing sand transport between the dune foot and the dune crest, we see that the depth-integrated sediment flux at the dune foot decreases as a function of absolute wind direction, with more transport the closer the wind direction approaches shore-parallel (Figure 10a, positions 1). In contrast, the transport magnitude at the dune crest is much closer related to the wind magnitude, with the exception of increased transport at d4 which is more oblique but has lower wind speed than d2 (Figure 10a,
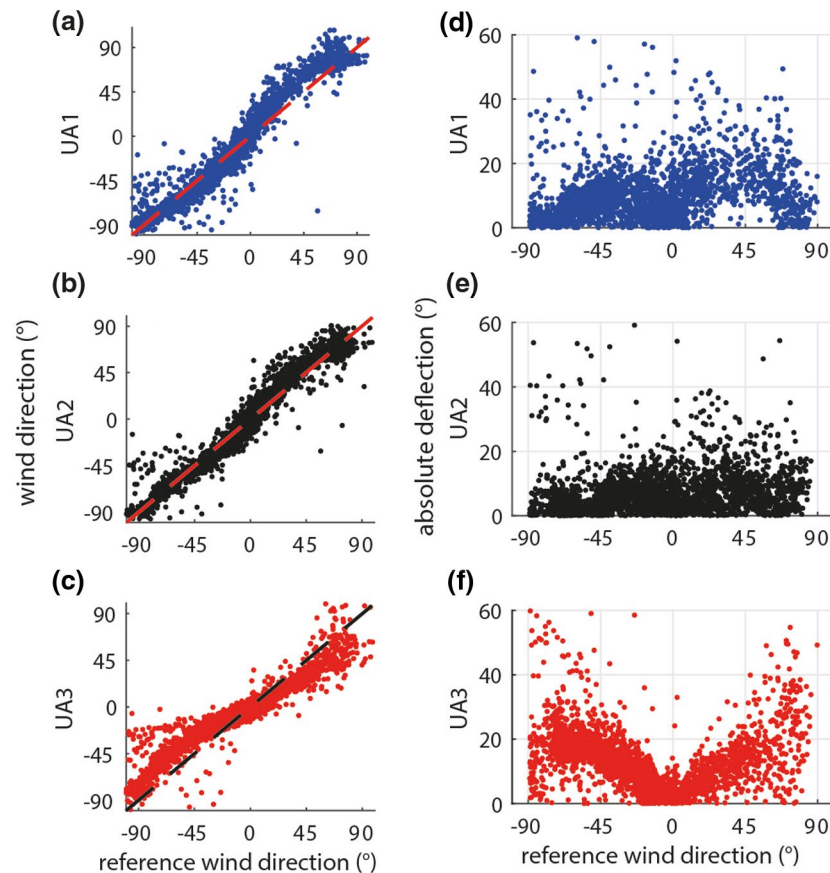
Figure 6. Wind direction across the foredune relative to the reference direction (a–c), absolute deflection angle relative to the reference wind direction (d–f).

positions 3). Our sediment transport measurements, although carried out over only 5 days took place during wind velocities and directions, representative for the month October (Figure 10b) and the whole year of 2017 (data not shown).

4.3. Vegetation and Morphology

At the study transect, all common species were observed (marram grass, sand couch, lesser hawkbit and sea rocket). Sand couch grass was the dominant species around the dune foot (−46 to −53 m), whereas the lower, the upper foredune slope and crest were characterized by a dense cover of marram grass. Maximum vegetation cover was found at the crest. Vegetation cover increased linearly from the upper dune foot to the dune crest (Figure 9, cross-shore distance −53 to −72 m).

The total volume change during the study period was positive for the measured transect, with 3.64 m^3 m^{-1} from dune foot to dune crest. This is quite a substantial gain, as it constitutes almost 25% of the typical annual gain at Egmond (Donker et al., 2018). In more detail, the elevation change varied across the foredune (Figure 9) showing sand accumulation around the dune foot with a maximum of 0.17 m (−35 to −46 m), followed by erosion of 0.1 m at the upper dune foot (−46 to −53 m). Subsequently, sand accumulated up to 0.13 m on the lower slope (−53 to −60 m) followed by accretion of about 0.05 m on the upper slope (−60 to −70 m). The foredune crest eroded up to 0.31 m (−70 to −75 m).

A comparison between morphological change and vegetation cover erosion at the dune foot alternates with sedimentation (with a maximum of 0.13 m) as vegetation density increased from 20% to 51% (−53 to −60 m). Above 12 m the vegetation cover remained higher than 60% and was associated with a smaller elevation increase of 5 cm. A vegetation cover of 95% (or more) occurred simultaneously with maximal erosion
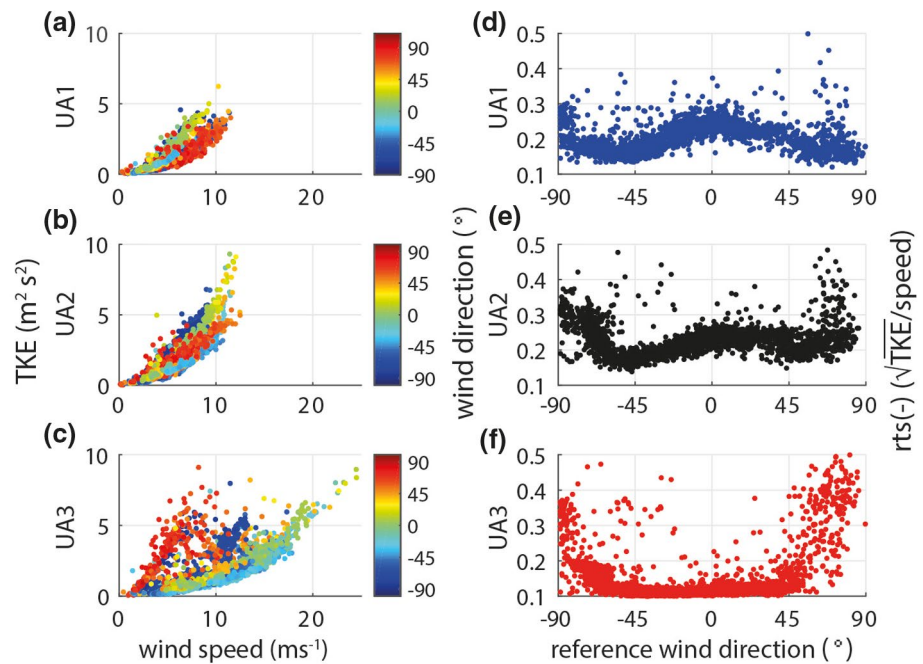
Figure 7. *TKE* and *rts* (−) in dependency to different wind speeds and wind-directions, (a–c), *TKE* relative to wind speed at three location across the foredune, color shows wind direction at the reference; (d–f) *rts* (√(*TKE*)/wind speed) at three locations across the foredune; Onshore flow is 0°, alongshore northern flow is 90°, alongshore southern flow is −90°.

at 18 m above mean sea level (Figure 9). At the bare dune foot, relatively large sand transport was recorded, together with a positive elevation change. On the upper dune foot, just below the vegetation edge (at −52 m distance from reference), the largest sand transport was found with 305% but at the same time erosion was observed. On the dune slope the vegetation cover increased and the mass flux decreased to 16.8%, while elevation increased by 0.13 m. At the dune crest where the vegetation cover was 100%, hardly any sand transport was observed (SC3), but the most erosion was observed (Figure 9).

5. Discussion

This study investigates the relative influence of sediment availability from the beach and vegetation altered transport capacity across the foredune on foredune growth and recovery. We hypothesized that sediment deposition across the foredune is governed by both the transport path across the vegetated foredune which is dependent on wind direction, topographic steering and sediment input from the beach. In this section we put the results of our wind, sand flux and vegetation cover analyses in context with existing literature, building up to the actual test of our hypothesis.

5.1. Wind

We measured direction and foredune location dependent wind flow deflection and alteration. At the dune foot incoming winds deflected toward alongshore directions, with maximum wind deflection at oblique wind directions of 30°–70°. Maximum wind deceleration and acceleration (between dune-foot and lower slope) was observed at highly oblique (>60°) and shore perpendicular (0°) wind directions, respectively (Figures 2, 5, and 6). We observed considerable wind acceleration across the dune slope (UA1-UA3), with a maximum of 3.1-fold acceleration during shore perpendicular wind. At the dune crest we observed deflection toward shore perpendicular directions, with maximum deflection at highly oblique wind directions (>60°) (UA3) (Figures 2, 5, and 6). These findings agree with previous studies investigating topographic steering at lower (10 m) foredunes (Bauer et al., 2012; P. A. Hesp et al., 2015; Walker & Hesp, 2013). The acceleration for onshore winds were most likely due to flow compression (P. A. Hesp et al., 2015; Walker
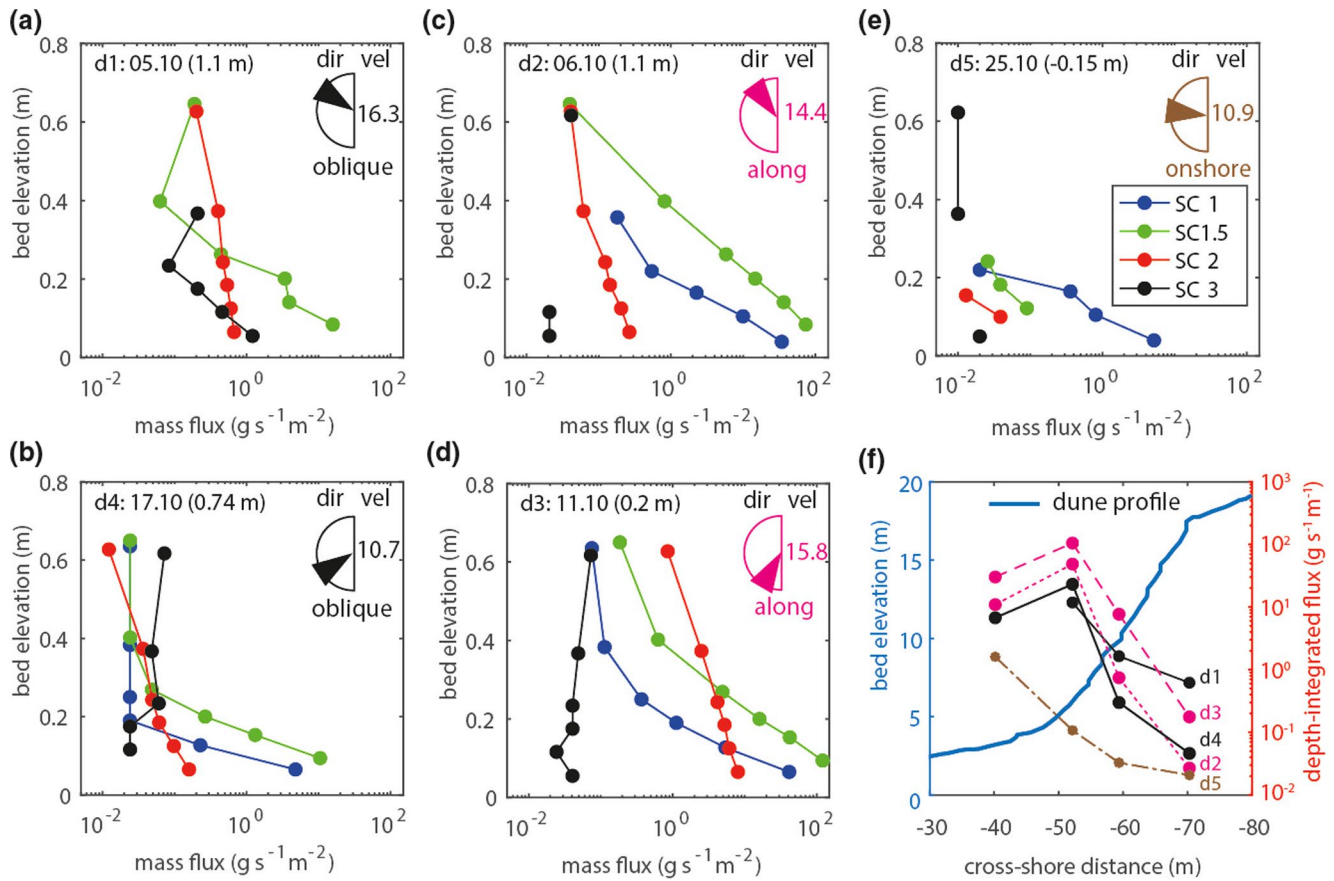
Figure 8. Sand transport flux across the foredune arranged by wind conditions (oblique, along, and onshore). (a–e) Sand transport flux profiles (g s^{-1} m^{-2}), d1–d5 indicates the day sediment transport was measured with the tidal stage relative to mean sea level in brackets, arrows (dir) indicates wind direction at reference, (vel) shows the 95th percentile of wind velocities at reference in m s^{-1}; (f) depth-integrated sand transport flux (g s^{-1} m^{-1}) across the foredune for d1–d5.
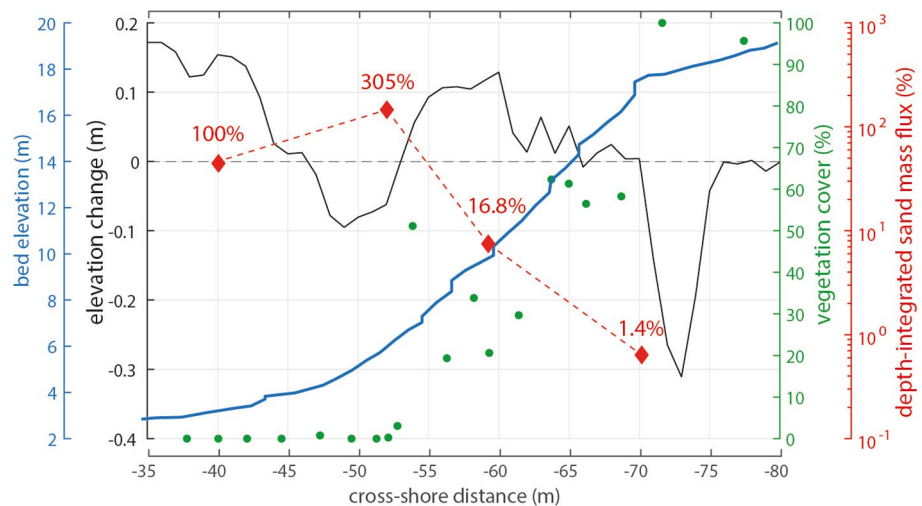

Figure 9. Vegetation changes in morphology and sand transport across the foredune over the measurement period, (blue) dune profile, (black) elevation change over our measurement campaign, (red) mean sand flux over measurement campaign, (green) vegetation cover in percent.
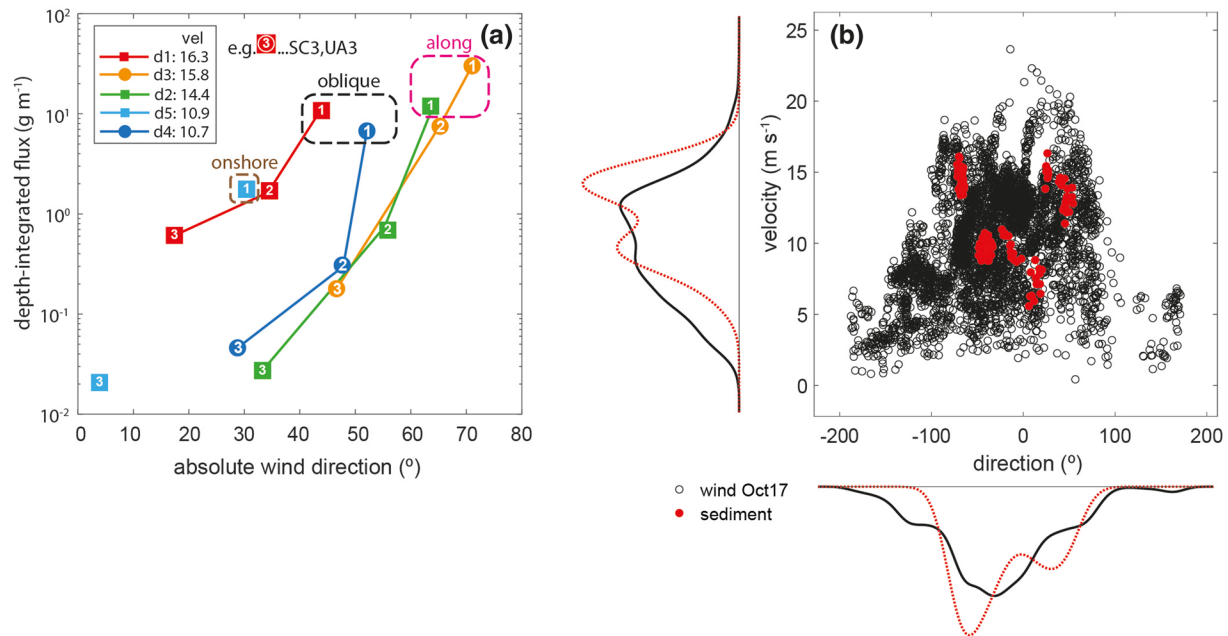
Figure 10. Panel (a) shows the depth-integrated sediment transport flux as a function of abs. wind-direction, (0° = onshore and 90° = alongshore), colors red to blue indicate wind velocity magnitude from high to low, numbers indicate position across the foredune measuring both sediment flux and velocity, 1 = dune foot, 2 = upper slope, and 3 = dune crest, at the dune foot (1s) more along-shore wind directions instigate higher sediment transport fluxes, at the dune crest (3s) wind velocity seems the main determinant of the sediment transport flux; panel (b) shows distribution in wind velocity and direction during sediment measurements (red) is a good representation of October 2017 (black) and all of 2017 (data not shown).

et al., 2017). A shift between oblique onshore (−45 and 45°) to shore perpendicular onshore (<22°) winds resulted in up to 3 times higher flow acceleration. In contrast, P. A. Hesp et al. (2015) found that flow would accelerate by a factor of 1.25 in a CFD model. The larger acceleration in the present study could be due to the larger dune height. The doubling in dune height could be an explanation for a more pronounced streamline compression and accordingly higher acceleration for onshore winds; however, other findings show that the magnitude of acceleration (ca. 1.5 times) is of the same order for a 10 and 23 m dune, which is attributed to an increased roughness (by vegetation) and deflection of flow (Arens et al., 1995). Arens et al. (1995) measured wind flows, however, at a higher location above the bed than the 0.9 m used in this study and over a dune with a steepness of approximately 1:5 (11.3°). Considering the large speed up across the foredune in Egmond, it is difficult to disentangle the effect of increased roughness by vegetation and topographic steering. The steeper foredune slope of 1:2.5 (21.8°) in this study could have been the reason for increased acceleration, because flow compression was largest at the upper half of the dune slope. This could become the subject of future CFD modeling investigations.

Due to the variety of the measured wind directions, ranging from northern to southern alongshore wind directions, we could observe a small asymmetry in topographic steering and acceleration. Southern oblique incipient winds (<−30°) experienced slightly increased topography steering at the crest and slightly reduced topographic steering at the dune foot, which was reversed for northern oblique incipient winds (>30°) (Figure 6). Moreover, topographic steering led to a lower velocity of northern alongshore winds than for their southern counterparts (Figure 5). This could be related to differences in gustiness of the winds originating from different directions.

We observed an increase in *TKE* with increasing wind velocities with highest values of 3.0 $m^2 s^2$ at the dune foot (wind 10–15 m s^{-1}), 5.3 $m^2 s^2$ at mid-slope (wind 10–15 m s^{-1}), and 3.5 $m^2 s^2$ at the crest (wind 15–20 m s^{-1}). These values are comparable to *TKE* values of 1.8–3.4 $m^2 s^2$ for wind velocities of 8–15 m s^{-1} measured by Hesp et al. (2013) at the dune foot and mid-slope of Prince Edward Island, Canada. We observed a wind-direction dependency on the rate of *TKE* growth with wind velocity. At the dune foot, the TKE of perpendicular and slightly oblique wind (< ± 30°) increased faster with increasing velocity. At the dune crest this pattern was reversed, with *TKE* increasing much faster with velocity for alongshore wind than oblique

and shore perpendicular wind (Figures 7a–7c). This can also be observed using the dimensionless factor *rts*. At the dune foot, relatively higher turbulence could be found during perpendicular winds, whereas highly oblique incipient wind directions cause dominant turbulence at mid-slope and the dune crest (Figure 7). This trend was also found in Chapman et al. (2013). When taking the velocity dependency into account by calculating *rts* values for their results, the *rts* was largest for smaller wind velocities (4–7.5 m s^{-1}) and larger at the dune foot. Like the asymmetry of changes in wind speed and direction, the turbulent flows were not symmetrical for the same approaching wind directions. When wind originated from northern directions, the *rts* was larger than for the respective southern directions. This is most likely because northern winds during the study period were inherent more turbulent, based on available wind gust data. Wind gusts, computed as the highest instantaneous U in the 3-s smoothed time series, were larger for northern than southern onshore winds at all three UAs (not shown).

5.2. Sand Transport

Measured height-integrated sand transport mass fluxes varied considerably in response to the incoming wind direction as well as across the foredune. From dune foot to the crest sand fluxes decreased on average by 99% (Figure 8). This rapid reduction was also found during previous studies (Arens, 1996; Arens & van der Lee, 1995; Davidson-Arnott et al., 2012; Petersen et al., 2011). The different transport events measured were characterized by varying wind directions and magnitudes, among which wind directions seemed to play a governing role on sand transport across the foredune. Larger sand transport was measured for stronger winds that approached the coast obliquely or were shore-parallel. The importance of wind directions was, for example compared by similar wind conditions with different obliqueness (d1 and d3). Increasing obliqueness (d3) resulted in increased transport at the lower and upper slope but lower transport at the dune crest (Figures 8a and 8c). Moreover, a comparison of d1 and d2 shows that, although the wind velocity of d1 is larger than d2, the increased obliqueness of d2 results in higher transport at dune foot and lower transport at the dune crest (Figures 8a and 8b). The strong dependence on wind direction is consistent with video observations of aeolian activity at Egmond beach (Hage et al., 2018), in which strong activity, visible through the presence and migration of aeolian bedforms known as sand strips, was observed during oblique and alongshore winds only. Furthermore, surface moisture observations (Smit et al., 2019) and modeling (Hage et al., 2020) indicated that most of the intertidal beach at Egmond may remain too wet to facilitate the initiation of aeolian transport. Thus, we believe that the larger transports at d3 relative to d1 are predominantly due to the more oblique winds at d3, not to the lower tidal stage (0.2 vs. 1.1 m) and hence wider beach. The dependence of sand transport mass fluxes on wind direction suggests transport limitations due to the fetch effect during shore-perpendicular winds, consistent with fetch-based modeling results in Hage et al. (2020).

The above presented measurements only constitute results of one cross-shore transect. This raises the question on how representative the observed sand transport and morphological development is for a larger alongshore region. A comparison between the elevation change of the measurement transect and the average elevation change over a ~1 km longshore distance reveals that observed sedimentation and erosion patterns at the cross-shore transect match with alongshore averaged cross-shore trend (Figures 11a and 11b). Moreover, measured gradients in depth-integrated sediment fluxes at the measurement transect can be set into context with the long shore variability. A volume gain of 3.64 m^3 m^{-1} was recorded at the measurement transect, which is 96% of the median alongshore gain in dune volume during our measurement campaign (Figure 11c).

The observed dependence of the cross-shore gradient in the vertically integrated mass flux Q_m on the wind direction (Figure 8) may have substantial consequences for how an eroded scarped foredune recovers. During shore-perpendicular winds Q_m was observed to be largest at the dune foot, which will lead to local deposition. During oblique and alongshore winds, the mass flux was highest well above the dune foot, just below the start of the vegetation, implying that these winds are responsible for bringing the sand higher up on the foredune. At a vegetation cover of 50% most of the sand was deposited at the foredune stoss slope. This cover is in the same range as reported in earlier studies. For example, Arens (1996) stated that vegetation densities of 20%–30% are sufficient to trap the majority of wind-blown sand. However, our results further show that sediment deposition within the foredune is not only a function of vegetation density and sediment input
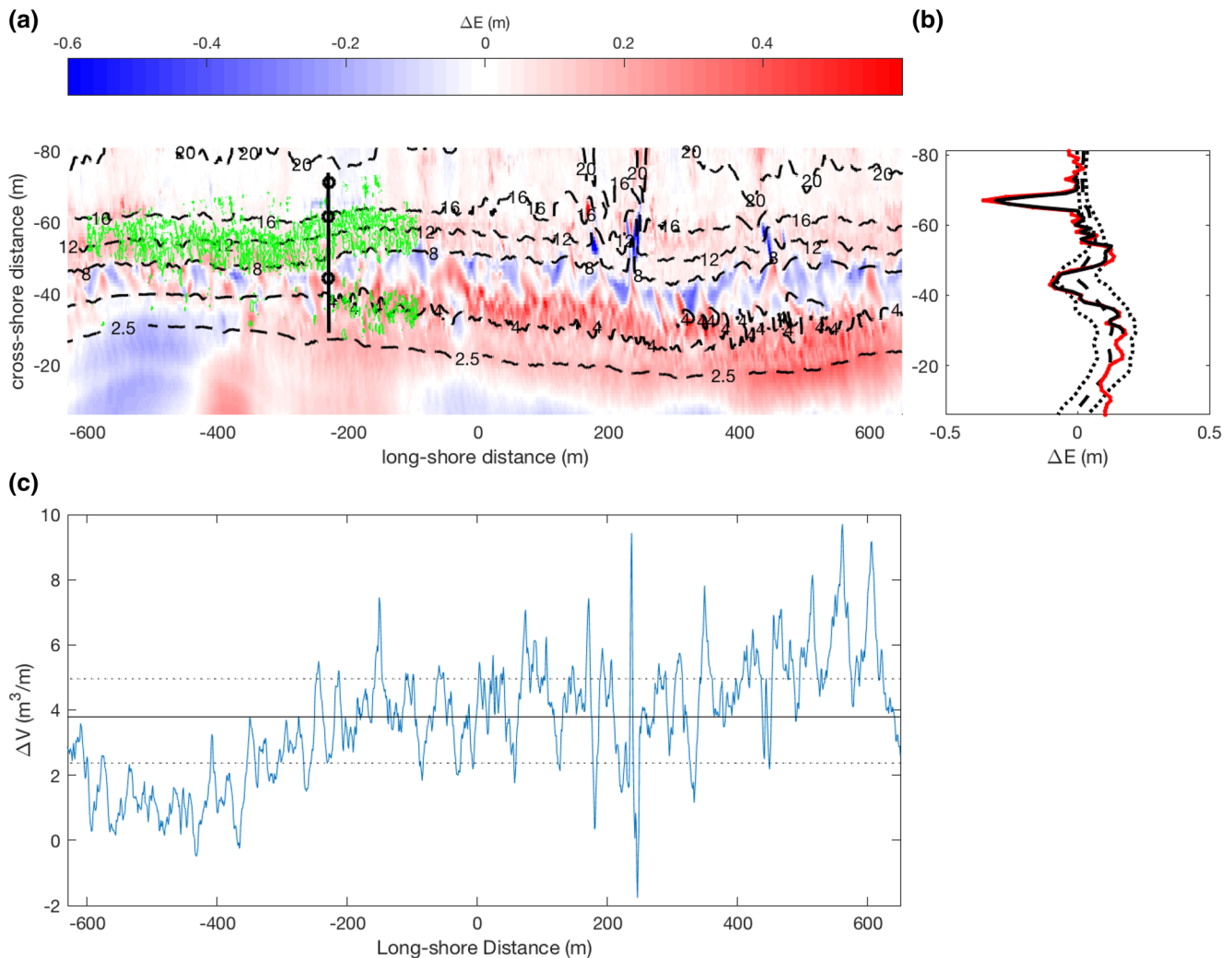
Figure 11. Morphological change at and around the measurement transect. (a) Bed elevation difference map of the field campaign based on UAV lidar surveys of 3 November 2017 and 23 August 2017, ΔE shows the difference in elevation, where positive/negative numbers mean sedimentation/erosion, respectively. The vertical black line is the position of the measurement transect, and the black circles are UA positions. Black contour lines show the foredune elevation after our field campaign, the green contour line shows vegetation edge. (b) Along shore median difference elevation (dashed), 25th and 75th percentiles (pointed), measurement transect RTK (black line), measurement transect difference lidar surveys (red line); (c) ΔV, change in dune volume during the field campaign, calculated from the dune foot (2.5 m + MSL, mean sea level) to the change in dune-slope at the upper slope. Solid line shows the median, the dashed lines are the 25th and 75th percentiles. We used to 2.5 m + MSL to calculate the dune volume since this was the highest waterlevel estimated on the beach Tuijnman et al. (2020).

from the beach, but also more importantly of topographic steering, which determines the transport limitations across the foredune face. We would therefore suggest that small foredunes display similar growth at the dune crest during shore-parallel and weak obliques winds, while high foredunes exhibit relatively more dune growth during oblique winds due to differences in topographic steering. These new insights might not only be able to help understand foredune recovery and the difference in observations between modeled and observed foredune growth (Davidson-Arnott et al., 2018; Duran & Moore, 2013). They will also help interpreting long-term field measurements on foredune sedimentation (e.g., Keijsers et al., 2015), providing a framework to distinguish the role of vegetation and topographic steering on foredune development.

In summary, our measurements indicate that sediment transport at the foredune foot is governed by wind-direction dependent fetch limitation (Figure 10a). In contrast, sediment transport at the foredune crest, and thus dune growth is more dependent on incoming velocity and obliqueness altering transport capacity. Thus, weak, oblique winds cause more transport at the crest than stronger, shore-parallel winds

(i.e., d4, d2 in Figure 10a). We suggest this is caused by the increased projected length aeolian sediments need to travel through the vegetated foredune and its accompanying loss in velocity and transport capacity. Given the representativeness of the measured transport conditions in our study this has also implications on foredune growth (Figure 10b). In contrast to the suggestion of Davidson-Arnott et al., (2018) that foredune growth is mainly dependent on sediment availability at the beach, our results indicate that also wind magnitudes and density/length of the vegetation cover will impact dune growth.

6. Conclusions

Our study shows the importance of wind direction and vegetation cover on aeolian mass flux patterns and the recovery of an eroded, steep (1:2.5, 21.8°) and high (~20 m) foredune stoss slope. Consistent with earlier studies, shore-perpendicular winds result in the largest wind acceleration from the dune foot to the crest (here, by a factor of 3), and a reduction in aeolian mass flux over the same distance. The rapid decrease in the flux toward the crest will lead to deposition at the dunefoot. We could, moreover, show that larger aeolian mass fluxes at the dune foot during oblique winds suggest fetch-induced transport limitations during cross-shore winds, however the dependence of aeolian transport fluxes on wind obliqueness at the dune crest suggests a limitation in transport capacity due to vegetation friction. Thus, transport limitation at the dune foot is induced by sediment availability, whereas transport limitation at the dune crest is induced by transport capacity, which depends on the incoming wind and the distance traveled over vegetation. Our study thus highlights the importance of wind direction and vegetation cover as important variables steering foredune recovery and growth.

Data Availability Statement

The UAV-Lidar data are available from Ruessink et al. (2019; doi:https://doi.org/10.5281/zenodo.2635416). All wind, sand transport and vegetation data are available on the Zenodo repository (doi: 10.5281/zenodo.4270358).

References

Aagaard, T., Kroon, A., Andersen, S., Sørensen, R. M., Quartel, S., & Vinther, N. (2005). Intertidal beach change during storm conditions; Egmond, the Netherlands. *Marine Geology*, *218*(1–4), 65–80. https://doi.org/10.1016/j.margeo.2005.04.001

Arens, S. M. (1996). Rates of aeolian transport on a beach in a temperate humid climate. *Geomorphology*, *17*(1–3), 3–18. https://doi.org/10.1016/0169-555X(95)00089-N

Arens, S. M., van Boxel, J. H., & Abuodha, J. O. Z. (2002). Changes in grain size of sand in transport over a foredune. *Earth Surface Processes and Landforms*, *27*(11), 1163–1175. https://doi.org/10.1002/esp.418

Arens, S. M., & van der Lee, G. E. M. (1995). Saltation sand traps for the measurement of aeolian transport into the foredunes. *Soil Technology*, *8*(1), 61–74. https://doi.org/10.1016/0933-3630(95)00007-5

Arens, S. M., Van Kaam-Peters, H. M. E., Van Boxel, J. H., Van Kaam-Peters, H. M. E., & Van Boxel, J. H. (1995). Air flow over foredunes and implications for sand transport. *Earth Surface Processes and Landforms*, *20*(4), 315–332. https://doi.org/10.1002/esp.3290200403

Bagnold, R. A. (1954). *The physics of blown sand and desert dunes*. London, UK: Methuen.

Bauer, B. O., & Davidson-Arnott, R. G. D. (2002). A general framework for modeling sediment supply to coastal dunes including wind angle, beach geometry, and fetch effects. *Geomorphology*, *49*(1), 89–108. https://doi.org/10.1016/S0169-555X(02)00165-4

Bauer, B. O., Davidson-Arnott, R. G. D., Walker, I. J., Hesp, P. A., & Ollerhead, J. (2012). Wind direction and complex sediment transport response across a beach-dune system. *Earth Surface Processes and Landforms*, *37*(15), 1661–1677. https://doi.org/10.1002/esp.3306

Carter, R. W. G., Hesp, P. A., & Nordstrom, K. F. (1990). Erosional landforms in coastal dunes. In K. F., Nordstrom, N. P., Psuty, & R.W.G., Carter (Eds.), *Coastal dunes. Form and process* (pp. 217–250). London, UK: Wiley.

Carter, R. W. G., & Stone, G. W. (1989). Mechanisms associated with the erosion of sand dune cliffs, Magilligan, Northern Ireland. *Earth Surface Processes and Landforms*, *14*(1), 1–10. https://doi.org/10.1002/esp.3290140102

Castelle, B., Bujan, S., Ferreira, S., & Dodet, G. (2017). Foredune morphological changes and beach recovery from the extreme 2013/2014 winter at a high-energy sandy coast. *Marine Geology*, *385*, 41–55.

Chapman, C., Walker, I. J., Hesp, P. A., Bauer, B. O., Davidson-Arnott, R. G. D., & Ollerhead, J. (2013). Reynolds stress and sand transport over a foredune. *Earth Surface Processes and Landforms*, *38*(14), 1735–1747. https://doi.org/10.1002/esp.3428

Christiansen, M. B., & Davidson-Arnott, R. (2004). Rates of landward sand transport over the foredune at Skallingen, Denmark and the role of dune ramps. *Geografisk Tidsskrift*, *104*(1), 31–43. https://doi.org/10.1080/00167223.2004.10649502

Cohn, N., Ruggiero, P., de Vries, S., & Kaminsky, G. M. (2018). New insights on coastal foredune growth: The relative contributions of Marine and aeolian processes. *Geophysical Research Letters*, *45*(10), 4965–4973. https://doi.org/10.1029/2018GL077836

Davidson-Arnott, R. G. D., Bauer, B. O., Walker, I. J., Hesp, P. A., Ollerhead, J., & Chapman, C. (2012). High-frequency sediment transport responses on a vegetated foredune. *Earth Surface Processes and Landforms*, *37*(11), 1227–1241. https://doi.org/10.1002/esp.3275

Davidson-Arnott, R., Hesp, P., Ollerhead, J., Walker, I., Bauer, B., Delgado-Fernandez, I., & Smyth, T. (2018). Sediment budget controls on foredune height: Comparing simulation model results with field data. *Earth Surface Processes and Landforms*, *43*(9), 1798–1810. https://doi.org/10.1002/esp.4354

Davidson-Arnott, R. G. D., MacQuarrie, K., & Aagaard, T. (2005). The effect of wind gusts, moisture content and fetch length on sand transport on a beach. *Geomorphology*, *68*(1–2), 115–129. https://doi.org/10.1016/j.geomorph.2004.04.008

Davidson-Arnottt, R. G. D., & Law, M. N. (1996). Measurement and prediction of long-term sediment supply to coastal foredunes. *Journal of Coastal Research*, (Vol 12), 654–663. https://doi.org/10.2307/4298513

De Winter, W., Donker, J., Sterk, G., Van Beem, G. J., & Ruessink, G. (2020). Regional versus local wind speed and direction at a narrow beach with a high and steep foredune. *PLoS ONE*, *15*(1), e0226983. https://doi.org/10.1371/journal.pone.0226983

De Winter, R. C., Gongriep, F., & Ruessink, B. G. (2015). Observations and modeling of alongshore variability in dune erosion at Egmond aan Zee, the Netherlands. *Coastal Engineering*, *99*, 167–175. https://doi.org/10.1016/j.coastaleng.2015.02.005

De Winter, W., van Dam, D. B., Delbecque, N., Verdoodt, A., Ruessink, B. G., & Sterk, G. (2018). Measuring high spatiotemporal variability in saltation intensity using a low-cost Saltation Detection System: Wind tunnel and field experiments. *Aeolian Research*, *31*, 72–81. https://doi.org/10.1016/J.AEOLIA.2017.11.003

Delgado-Fernandez, I. (2010). A review of the application of the fetch effect to modelling sand supply to coastal foredunes. *Aeolian Research*, *2*, 61–70. https://doi.org/10.1016/j.aeolia.2010.04.001

Delgado-Fernandez, I. (2011). Meso-scale modelling of aeolian sediment input to coastal dunes. *Geomorphology*, *130*, 230–243.

Dong, Z., Lu, J., Man, D., Lv, P., Qian, G., Zhang, Z., & Luo, W. (2011). Equations for the near-surface mass flux density profile of wind-blown sediments. *Earth Surface Processes and Landforms*, *36*(10), 1292–1299. https://doi.org/10.1002/esp.2151

Donker, J., van Maarsseveen, M., & Ruessink, G. (2018). Spatio-temporal variations in foredune dynamics determined with mobile laser scanning. *Journal of Marine Science and Engineering*, *6*(4), 126. https://doi.org/10.3390/jmse6040126

Duran, O., & Moore, L. J. (2013). Vegetation controls on the maximum size of coastal dunes. *Proceedings of the National Academy of Sciences*, *110*(43), 17217–17222. https://doi.org/10.1073/pnas.1307580110

Ellis, J. T., Li, B., Farrell, E. J., & Sherman, D. J. (2009). Protocols for characterizing aeolian mass-flux profiles. *Aeolian Research*, *1*(1–2), 19–26.

Goossens, D., & Offer, Z. Y. (2000). Wind tunnel and field calibration of six aeolian dust samplers. *Atmospheric Environment*, *34*(7), 1043–1057. https://doi.org/10.1016/S1352-2310(99)00376-3

Hage, P., Ruessink, G., & Donker, J. (2018). Using Argus video monitoring to determine limiting factors of aeolian sand transport on a narrow beach. *Journal of Marine Science and Engineering*, *6*, 138. https://doi.org/10.3390/jmse6040138

Hage, P., Ruessink, G., Van Aartrijk, Z., & Donker, J. (2020). Using video monitoring to test a fetch-based aeolian sand transport model. *Journal of Marine Science and Engineering*, *8*, 110. https://doi.org/10.3390/jmse8020110

Hesp, P. (1989). A review of biological and geomorphological processes involved in the initiation and development of incipient foredunes. *Proceedings of the Royal Society of Edinburgh Section B: Biological Sciences*, *96*, 181–201. https://doi.org/10.1017/S0269727000010927

Hesp, P. (2002). Foredunes and blowouts: Initiation, geomorphology and dynamics. *Geomorphology*, *48*(1–3), 245–268. https://doi.org/10.1016/S0169-555X(02)00184-8

Hesp, P. A., Davidson-Arnott, R., Walker, I. J., & Ollerhead, J. (2005). Flow dynamics over a foredune at Prince Edward Island, Canada. *Geomorphology*, *65*(1–2), 71–84. https://doi.org/10.1016/J.GEOMORPH.2004.08.001

Hesp, P. A., & Smyth, T. A. G. (2016a). Jet flow over foredunes. *Earth Surface Processes and Landforms*, *41*(12), 1727–1735. https://doi.org/10.1002/esp.3945

Hesp, P. A., & Smyth, T. A. G. (2016b). Surfzone–beach–dune interactions: Flow and sediment transport across the intertidal beach and backshore. *Journal of Coastal Research*, *75*(special issue), 8–12.

Hesp, P. A., & Smyth, T. A. (2019). CFD flow dynamics over model scarps and slopes. *Physical Geography*, 1–24.

Hesp, P. A., Smyth, T. A. G., Nielsen, P., Walker, I. J., Bauer, B. O., & Davidson-Arnott, R. (2015). Flow deflection over a foredune. *Geomorphology*, *230*, 64–74. https://doi.org/10.1016/j.geomorph.2014.11.005

Hesp, P. A., & Walker, I. J. (2013). Coastal dunes. In J. Shroder, N. Lancaster, D. J. Sherman & A. C. W. Bass (Eds.), *Treatise on geomorphology* (Vol. 11, pp. 328–355). San Diego, CA: Academic Press. https://doi.org/10.1016/B978-0-12-374739-6.00310-9

Hesp, P. A., Walker, I. J., Chapman, C., Davidson-Arnott, R., & Bauer, B. O. (2013). Aeolian dynamics over a coastal foredune, Prince Edward Island, Canada. *Earth Surface Processes and Landforms*, *38*(13), 1566–1575. https://doi.org/10.1002/esp.3444

Hoonhout, B. M., & de Vries, S. (2016). A process-based model for aeolian sediment transport and spatiotemporal varying sediment availability. *Journal of Geophysical Research: Earth Surface*, *121*(8), 1555–1575. https://doi.org/10.1002/2015JF003692

Keijsers, J. G. S., De Groot, A. V., & Riksen, M. J. P. M. (2015). Vegetation and sedimentation on coastal foredunes. *Geomorphology*, *228*(2015), 723–734.

Maun, M. A. (1998). Adaptations of plants to burial in coastal sand dunes. *Canadian Journal of Botany*, *76*(5), 713–738. https://doi.org/10.1139/b98-058

Maun, M. A. (2009). *The biology of coastal sand dunes*. Oxford University Press.

Ollerhead, J., Davidson-Arnott, R., Walker, I. J., & Mathew, S. (2013). Annual to decadal morphodynamics of the foredune system at Greenwich Dunes, Prince Edward Island, Canada. *Earth Surface Processes and Landforms*, *38*(3), 284–298. https://doi.org/10.1002/esp.3327

Petersen, P. S., Hilton, M. J., & Wakes, S. J. (2011). Evidence of aeolian sediment transport across an Ammophila arenaria-dominated foredune, Mason Bay, Stewart Island. *New Zealand Geographer*, *67*(3), 174–189. https://doi.org/10.1111/j.1745-7939.2011.01210.x

Piscioneri, N., Smyth, T. A., & Hesp, P. A. (2019). Flow dynamics over a foredune scarp. *Earth Surface Processes and Landforms*, *44*(5), 1064–1076.

Psuty, N. (2008). The coastal foredune: A morphological basis for regional coastal dune development. *Coastal Dunes*, 11–27.

Ruessink, G., Schwarz, C. S., Price, T. D., & Donker, J. J. A. (2019). A Multi-year data set of beach-foredune topography and environmental forcing conditions at Egmond aan Zee, the Netherlands. *Data*, *4*(2), 73. https://doi.org/10.3390/data4020073

Short, A. D. D., & Hesp, P. A. A. (1982). Wave, beach and dune interactions in Southeastern Australia. *Marine Geology*, *48*(3–4), 259–284. https://doi.org/10.1016/0025-3227(82)90100-1

Smit, Y., Donker, J. J. A., & Ruessink, G. (2019). Spatiotemporal surface moisture variations on a barred beach and their relationship with groundwater fluctuations. *Hydrology*, *6*, 8. https://doi.org/10.3390/hydrology6010008

Smyth, T. A. G., Jackson, D. W. T., & Cooper, J. A. G. (2012). High resolution measured and modelled three-dimensional airflow over a coastal bowl blowout. *Geomorphology*, *177*, 62–73. https://doi.org/10.1016/j.geomorph.2012.07.014

Sterk, G., Parigiani, J., Cittadini, E., Peters, P., Scholberg, J., & Peri, P. (2012). Aeolian sediment mass fluxes on a sandy soil in Central Patagonia. *Catena*, *95*, 112–123. https://doi.org/10.1016/j.catena.2012.02.005

Sterk, G., & Raats, P. A. C. (1996). Comparison of Models describing the vertical distribution of wind-eroded sediment. *Soil Science Society of America Journal*, *60*(6), 1914. https://doi.org/10.2136/sssaj1996.03615995006000060042x

Tuijnman, J. T., Donker, J. J., Schwarz, C. S., & Ruessink, G. (2020). Consequences of a storm surge for aeolian sand transport on a low-gradient beach. *Journal of Marine Science and Engineering*, *8*(8), 584.

van Duin, M. J. P., Wiersma, N. R., Walstra, D. J. R., van Rijn, L. C., & Stive, M. J. F. (2004). Nourishing the shoreface: Observations and hindcasting of the Egmond case, the Netherlands. *Coastal Engineering*, *51*(8–9), 813–837. https://doi.org/10.1016/j.coastaleng.2004.07.011

Van Enckevort, I. M. J., & Ruessink, B. G. (2001). Effect of hydrodynamics and bathymetry on video estimates of nearshore sandbar position. *Journal of Geophysical Research: Oceans*, *106*(C8), 16969–16979.

Walker, I. J., Davidson-Arnott, R. G. D., Bauer, B. O., Hesp, P. A., Delgado-Fernandez, I., Ollerhead, J., & Smyth, T. A. G. (2017). Scale-dependent perspectives on the geomorphology and evolution of beach-dune systems. *Earth-Science Reviews*, *171*, 220–253. https://doi.org/10.1016/J.EARSCIREV.2017.04.011

Walker, I. J., Davidson-Arnott, R. G. D., Hesp, P. A., Bauer, B. O., & Ollerhead, J. (2009). Mean flow and turbulence responses in airflow over foredunes: New insights from recent research. *Journal of Coastal Research*, *2009*(56), 366–370. https://doi.org/10.2307/25737599

Walker, I. J., & Hesp, P. A. (2013). Fundamentals of aeolian sediment transport: Airflow over dunes. In *Treatise on geomorphology*. Vol. *11* (pp. 109–133). Elsevier. https://doi.org/10.1016/B978-0-12-374739-6.00300-6

Zarnetske, P. L., Hacker, S. D., Seabloom, E. W., Ruggiero, P., Killian, J. R., Maddux, T. B., & Cox, D. (2012). Biophysical feedback mediates effects of invasive grasses on coastal dune shape. *Ecology*, *93*(6), 1439–1450. https://doi.org/10.1890/11-1112.1